Acta Crystallographica Section C
Crystal Structure Communications
ISSN 0108-2701

Directed anisotropy in bis(acetato-κ^2O,O')diaquazinc(II) at 110 and 250 K

Martin Lutz* and Anthony L. Spek

Bijvoet Center for Biomolecular Research, Crystal and Structural Chemistry, Faculty of Science, Utrecht University, Padualaan 8, 3584 CH Utrecht, The Netherlands
Correspondence e-mail: m.lutz@uu.nl

Received 27 November 2008
Accepted 18 December 2008
Online 10 January 2009

The molecule of the title compound, $[Zn(C_2H_3O_2)_2(H_2O)_2]$, is located on a twofold axis in the crystal structure. The displacement parameters and the thermal expansion of the crystal show significant anisotropy. This is explained by the two-dimensional hydrogen-bonded structure, with only very weak interactions perpendicular to it. Besides the overall molecular motion, there are internal vibrations, which cause the Zn—O(carboxylate) bonds to fail the Hirshfeld rigid-bond test. It is shown that this can be interpreted in terms of the steric strain in the four-membered chelate ring due to the bidentate carboxylate coordination.

Comment

The room-temperature structure of the title compound, (I), is known from the literature (van Niekerk *et al.*, 1953; Semenenko & Kurdyumov, 1958; Kaduk & Chen, 1996; Ishioka *et al.*, 1997) to form a two-dimensional network by hydrogen bonding, with only very weak interactions in the third direction. The displacement ellipsoids show a large anisotropy and the Zn—O2 bond (Ishioka *et al.*, 1997) fails the Hirshfeld rigid-bond test (Hirshfeld, 1976) by 11σ, as calculated using *PLATON* (Spek, 2003). To investigate further the anisotropy of this compound, we performed temperature-dependent cell determinations and two complete crystal structure determinations at 110 and 250 K, denoted (I*a*) and (I*b*), respectively.

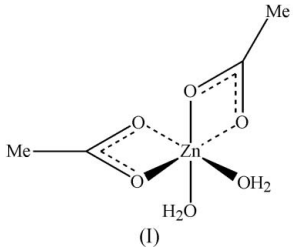

(I)

The Zn atom is located on a twofold rotation axis and has a distorted octahedral coordination environment, which is formed by four carboxylate O atoms and two water molecules

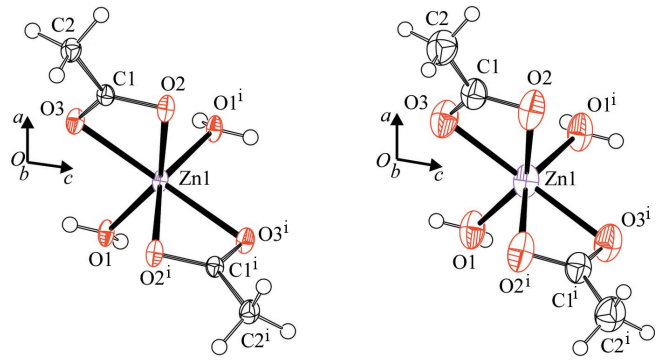

(I*a*) (I*b*)

Figure 1
Displacement ellipsoid plots and atomic numbering schemes for (I*a*) at 110 K and (I*b*) at 250 K. Ellipsoids are drawn at the 50% probability level and H atoms are shown as small spheres of arbitrary radii. [Symmetry code: (i) $-x, y, -z+\frac{1}{2}$.]

(Fig. 1). The plane of the water molecule makes an angle of 33 (2)° with the Zn1—O1 bond in (I*a*). This is in contrast with the trigonal coordination with an angle of 0.2 (6)° reported in the literature (Ishioka *et al.*, 1997, 1998). The Zn1—O1 bond to the coordinated water molecule is about 0.15 Å shorter than the Zn1—O2 and Zn1—O3 bonds to the carboxylate group (Tables 1 and 3). At 250 K, the latter Zn—O distances appear similar [(I*b*) data set], but at 110 K the difference of about 0.03 Å is significant [(I*a*) data set]. A large distortion from an ideal octahedron is found in the O—Zn—O angles, leading to angular distortions (Robinson *et al.*, 1971) of 248.4 (4) and 260.1 (5) degree^2 for (I*a*) and (I*b*), respectively.

The bidentate mode, in which both carboxylate O atoms coordinate to the same Zn centre and form a four-membered Zn—O—C—O ring, leads to an extremely strained situation, with Zn—O—C angles close to 90° instead of the optimal 120° and O—Zn—O angles close to 60° instead of the octahedral 90° (Tables 1 and 3). The Cambridge Structural Database (CSD, August 2008 update; Allen, 2002) contains 1052 carboxylate complexes of six-coordinated Zn. Only 241 of them have this bidentate coordination mode, of which 225 are not additionally bridging between different metals. The range of Zn—O distances is between 1.9359 (16) (Dietzel *et al.*, 2006) and 2.639 (4) Å (Tao *et al.*, 2000). Crystal structures of bidentate carboxylate groups with tetrahedral Zn centres are unknown.

The coordinated water molecule acts as donor in two intermolecular hydrogen bonds, with carboxylate atoms O2 and O3 as acceptors (Tables 2 and 4). This hydrogen bonding results in an infinite two-dimensional network in the crystallographic *bc* plane. Between the planes no strong interactions can be detected (van Niekerk *et al.*, 1953). The hydrogen-bonded sheet-like structure is also reflected in the morphology of the crystals, which are shaped as plates where the form {100} has the smallest dimension.

A rigid-body analysis of the displacement parameters using the program *THMA11* (Schomaker & Trueblood, 1998) results in a **TLS** model with weighted R values of 0.112 and 0.113 for (I*a*) and (I*b*), respectively (R = {[$\Sigma(w\Delta U)^2$]/

 doi:10.1107/S0108270108043242

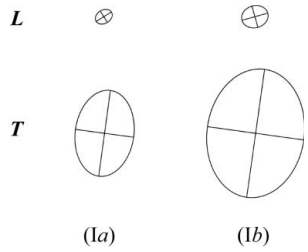

Figure 2
L and **T** tensors obtained from a rigid-body analysis for (I*a*) at 110 K and (I*b*) at 250 K. Views along the crystallographic *b* axis (same perspective as in Fig. 1). The eigenvalues of the **L** tensor are 3.24, 1.84 and 1.82 degree^2 for (I*a*), and 7.20, 4.91 and 3.20 degree^2 for (I*b*). The eigenvalues of the **T** tensor are 0.02309, 0.01048 and 0.00954 Å^2 for (I*a*), and 0.05150, 0.02877 and 0.02329 Å^2 for (I*b*). The eigenvectors $\mathbf{L}_1$ are in the *ac* plane and have angles to **a** of 57.93 and 74.25° for (I*a*) and (I*b*), respectively. The eigenvectors $\mathbf{T}_1$ are also in the *ac* plane and have angles to **a** of 7.45 and 7.72° for (I*a*) and (I*b*), respectively. The **S** tensors in (I*a*) and (I*b*) are (−0.00092, 0, 0.00037 / 0, 0.00079, 0 / 0.00049, 0, 0.00013) and (−0.00136, 0, 0.00055 / 0, 0.00152, 0 / 0.00090, 0, −0.00016) rad-Å.

$[\Sigma(wU_{obs})^2]\}^{1/2}$). The main axes of the **L** and **T** tensors are in the *ac* plane (Fig. 2). In particular, the **T** tensor is very anisotropic and the $\mathbf{T}_1$ axis is close to the *a* axis. Translational motion in the *b* and *c* directions is restricted due to the hydrogen-bonding network, while no such restriction exists in the *a* direction. Consistent with the rigid-body analysis, the displacement parameters of the individual atoms have their largest components in the direction of the *a* axis. For Zn1, the anisotropicity, defined as the ratio of the main axes $U3_{obs}/U1_{obs}$, is 2.57 in (I*a*) and 2.32 in (I*b*). The average anisotropicity of the whole molecule is 2.15 in (I*a*) and 1.94 in (I*b*).

While the average anisotropicity is covered by the calculated rigid-body model, with $U3_{calc}/U1_{calc}$ of 2.11 in (I*a*) and 1.87 in (I*b*), the displacement parameters of the individual atoms deviate significantly from this overall model. In other words, there is clearly additional internal motion (Fig. 3). Most affected is atom O2 of the carboxylate group and the O2—Zn1 bonds, which have large differences of mean-square displacement amplitudes (Δ m.s.d.a.'s) along the bond (Hirshfeld, 1976) of 0.0080 (5) and 0.0221 (7) Å^2 for (I*a*) and (I*b*), respectively. Internal motion also affects atom O3, but the effect is smaller than for atom O2, with Δ m.s.d.a.'s of 0.0026 (5) and 0.0017 (7) Å^2 for (I*a*) and (I*b*), respectively. These values can be compared with recent bidentate carboxylate complexes of octahedral Zn extracted from *Acta Crystallographica* (Table 5). Interestingly, all structures have at least one Zn—O(carboxylate) bond where the Hirshfeld rigid-bond test fails, with Δ m.s.d.a. larger than 0.01 Å^2 and/or Δ m.s.d.a./σ larger than 5. The similar bond lengths Zn1—O2 and Zn1—O3 observed by Ishioka *et al.* (1997) and also seen in (I*b*) should therefore be considered as an effect of vibrational smearing. It should also be noted that the standard uncertainties for atomic positions and displacement parameters are much higher in Ishioka *et al.* (1997) compared with (I*a*) and (I*b*). If (I*a*) is compared with (I*b*), it can easily be seen that cooling of the crystal does considerably reduce the effect of vibrational smearing, but even the 110 K structure of (I*a*)

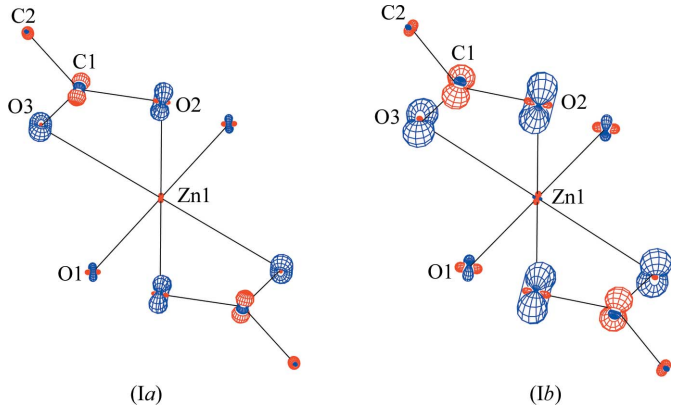

Figure 3
Peanut plots (Hummel *et al.*, 1990) of (I*a*) at 110 K and (I*b*) at 250 K, showing the difference between the measured displacement parameters and the **TLS** model from the program *THMA11* (Schomaker & Trueblood, 1998). A scale factor of 3.08 was used for the root-mean-square surfaces. Darker lines (blue in the electronic version of the paper) indicate positive differences and lighter lines (red in the electronic version) negative differences.

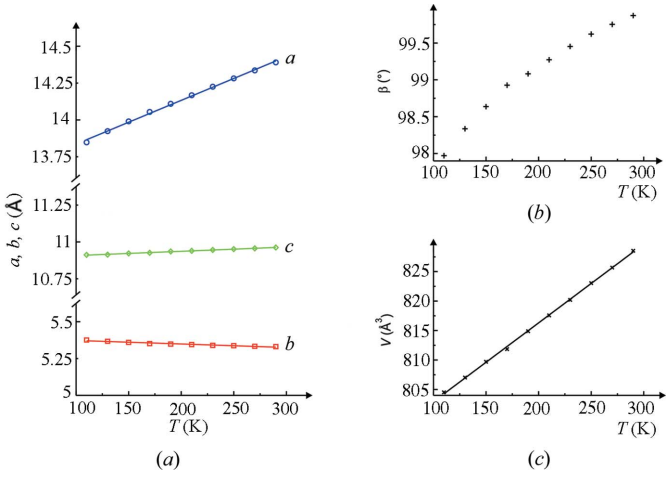

Figure 4
(*a*) Unit-cell length *a* (top), *b* (bottom) and *c* (middle), (*b*) cell angle *β* and (*c*) cell volume *V*, all as a function of temperature during cooling from 290 to 110 K at a cooling rate of 120 K h^{-1}. Each cell determination is based on a post-refinement (Schreurs, 2008) of 147–150 individual reflections (a = 13.539 + 2.97 × 10^{-3} T, b = 5.397 + 0.24 × 10^{-3} T, c = 10.879 + 0.29 × 10^{-3} T, V = 789.57 + 0.134 T).

still fails the Hirshfeld test. This might be attributed to the severe strain in the four-membered chelate ring, with bond angles deviating from ideal values (see above). An inspection of the internal movements in the four-membered ring (Fig. 3) suggests that these motions tend to release the strain. In anhydrous zinc acetate (Clegg *et al.*, 1986), there is no failure of the Hirshfeld test because the carboxylate group is bridging, with C—O—Zn angles in the normal range [113.0 (2)–134.6 (2)°], and the Zn atom is tetrahedral, with O—Zn—O angles also in the normal range [100.8 (1)–117.8 (1)°]. The latter conclusion can be generalized on the basis of 25 recently published crystal structures: bridging carboxylate groups usually fulfil the Hirshfeld test for Zn—O bonds in zinc complexes.

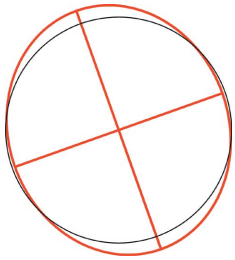

Figure 5
Strain ellipsoid of the thermal expansion between (I*a*) and (I*b*). The strain ellipsoid is defined by the equation $X_1^2/(1+\alpha_1\Delta T)^2 + X_2^2/(1+\alpha_2\Delta T)^2 + X_3^2/(1+\alpha_3\Delta T)^2 = 1$ (Küppers, 2003). View along the crystallographic *b* axis (same perspective as in Fig. 1). Shown in grey (red in the electronic version of the paper) is the deviation (greatly exaggerated) from isotropic behaviour (black). The corresponding eigenvalues α of the strain tensor are 253.9 (19.56° to **a**), −38.3 (27.51° to **c**) and −51.1 (parallel to **b**) 10^{-6} K^{-1}.

The large difference in the intermolecular bonding situation should result in a large anisotropy of the thermal expansion tensor (Salud *et al.*, 1998). We therefore performed a temperature-dependent study of the cell parameters by cooling the crystal from 290 to 110 K in steps of 20 K (Fig. 4). To minimize diffractometer errors in the cell determinations, we used the Phi/Phi-Chi routine (Duisenberg *et al.*, 2000) and kept the position of the detector fixed. The largest change is found for the *a* axis, which is the direction of the weakest intermolecular interactions. More details are obtained from an analysis of the thermal expansion tensor. Usually, the thermal expansion tensor is expressed in a Cartesian coordinate system, resulting in a symmetric second-rank tensor. With monoclinic symmetry, two off-diagonal terms of this tensor become zero, with one eigenvector parallel to the crystallographic twofold axis. The program *STRAIN* (Ohashi, 1982) was used for the calculation of the tensors and the results are shown in Tables 6 and 7. The eigenvalue of α_1 has the largest magnitude and is positive over the whole temperature range. α_1 is nearly collinear with the *a* axis. This can also be graphically visualized by a plot of the strain ellipsoid of the thermal expansion (Fig. 5). α_2 and α_3 have much smaller magnitudes. α_3 is parallel to the *b* axis by symmetry (see above) and has a negative sign over the whole temperature range. α_2 is also negative for most temperature changes. We can therefore conclude that the crystal has a biaxial negative thermal expansion as a consequence of the hydrogen-bonding pattern.

An alternative explanation for large displacement parameters is the choice of too high a space-group symmetry. The structure is then refined as an average and the corresponding increased displacement parameters are artefacts. Therefore, we performed a careful analysis of the symmetry. The crystal structure of (I) is best described in the centrosymmetric space group *C*2/*c*. In the literature there is a report of a refinement in *Cc*, which was unsuccessful due to abnormalities in the displacement parameters and the bond distances, which caused the authors to choose *C*2/*c* (Ishioka *et al.*, 1998). If the structure is solved in *P*1, the routine ADDSYM in *PLATON* (Spek, 2003) and the space group algorithm of *SUPERFLIP* (Palatinus & van der Lee, 2008) strongly suggest a transformation to *C*2/*c*. The correctness of *C*2/*c* is further proven by the least-squares refinement. The weakest reflections, which are most sensitive to the choice of the correct space group (Walker *et al.*, 1999), have a scale factor $K = [\mathrm{mean}(F_o^2)/\mathrm{mean}(F_c^2)]$ close to 1.0 (Table 8). If the real space group were noncentrosymmetric, a much higher value of *K* would be expected.

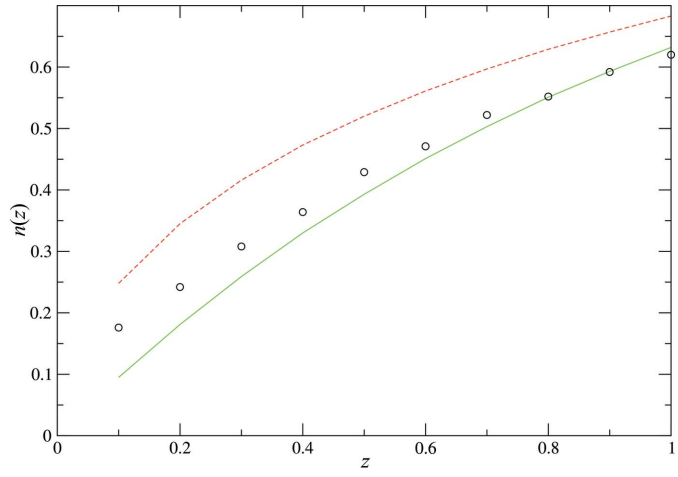

Figure 6
Cumulative $n(z)$ statistics for (I*a*), as calculated with the program *SIR97* (Altomare *et al.*, 1999). The experimental values are given as black circles. The theoretical curve for noncentrosymmetric structures is shown as a solid line and that for centrosymmetric structures as a dashed line.

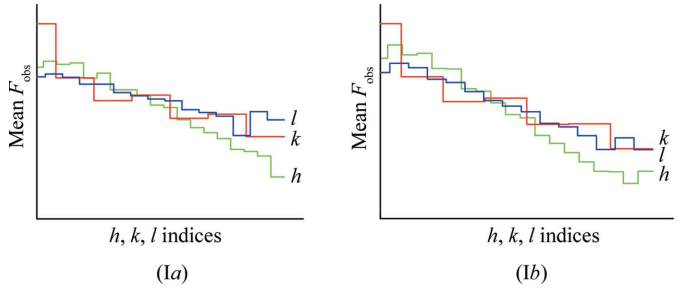

Figure 7
Mean intensities *versus* increasing index *h*, *k*, and *l* for (I*a*) and (I*b*), as calculated using the routine WTANAL in *WinGX* (Farrugia, 1999).

Nevertheless, the intensity statistics are noncentrosymmetric. $<|E^2 - 1|>$ for all reflections in (I*a*), as calculated using *SIR97* (Altomare *et al.*, 1999), is 0.798, with theoretical values of 0.968 for centrosymmetric and 0.736 for noncentrosymmetric structures. A cumulative $n(z)$ distribution is also indicative of a noncentrosymmetric structure (Fig. 6). A closer look shows that the Zn atoms on the special positions are the cause of the noncentrosymmetric intensity statistics. If $<|E^2 - 1|>$ is determined from calculated structure factors based only on Zn atoms, the result is 0.553, while calculated structure factors from only the C, H and O atoms lead to $<|E^2 - 1|>$ of 0.930.

Using the routine WTANAL of the *WinGX* package (Farrugia, 1999), it is possible to plot the mean intensities for the three principal directions of the crystal (Fig. 7). While similar behaviour is found for the *b** and *c** directions, the

intensity decay with resolution is significantly stronger in the a^* direction. This finding is consistent with the directions of the **T** tensor of the rigid-body analysis (see above). In accordance with this decay of Bragg intensities in the a^* direction, we expect the presence of diffuse intensity in this direction. This diffuse intensity can indeed be detected, but the effect is very weak: it was necessary to collect overexposed diffraction images at 250 K, different from the images of (I*b*), to make the streaks visible.

Experimental

Crystals of (I) were unintentionally obtained by slow evaporation of an aqueous solution of zinc acetate in the presence of urea in a molar ratio of 1:2 at room temperature.

Compound (I) at 110 K, (I*a*)

Crystal data

$[Zn(C_2H_3O_2)_2(H_2O)_2]$
M_r = 219.49
Monoclinic, $C2/c$
a = 13.8556 (2) Å
b = 5.38096 (7) Å
c = 10.92487 (14) Å
β = 97.942 (1)°
V = 806.71 (2) Å^3
Z = 4
Mo $K\alpha$ radiation
μ = 3.03 mm^{-1}
T = 110 (2) K
0.42 × 0.30 × 0.06 mm

Data collection

Nonius KappaCCD area-detector diffractometer
Absorption correction: numerical (*SADABS*; Sheldrick, 2008*a*)
T_{min} = 0.408, T_{max} = 0.856
6788 measured reflections
925 independent reflections
898 reflections with $I > 2\sigma(I)$
R_{int} = 0.015

Refinement

$R[F^2 > 2\sigma(F^2)]$ = 0.016
$wR(F^2)$ = 0.045
S = 1.10
925 reflections
60 parameters
H atoms treated by a mixture of independent and constrained refinement
$\Delta\rho_{max}$ = 0.35 e Å^{-3}
$\Delta\rho_{min}$ = −0.47 e Å^{-3}

Table 1
Selected geometric parameters (Å, °) for (I) at 110 K.

Zn1—O1	2.0076 (11)	O2—C1	1.2641 (18)
Zn1—O3	2.1653 (10)	O3—C1	1.2685 (17)
Zn1—O2	2.1962 (11)		
O1—Zn1—O1^{i}	98.81 (7)	O1—Zn1—O2^{i}	95.88 (4)
O1—Zn1—O3^{i}	106.92 (4)	O3—Zn1—O2^{i}	99.29 (4)
O1—Zn1—O3	90.37 (4)	O2—Zn1—O2^{i}	84.14 (6)
O3^{i}—Zn1—O3	153.57 (6)	C1—O2—Zn1	89.86 (8)
O1—Zn1—O2	149.71 (4)	C1—O3—Zn1	91.15 (8)
O3—Zn1—O2	59.95 (4)	O2—C1—O3	118.73 (13)

Symmetry code: (i) $-x, y, -z+\frac{1}{2}$.

Table 2
Hydrogen-bond geometry (Å, °) for (I) at 110 K.

D—H···A	D—H	H···A	D···A	D—H···A
O1—H1O···O2^{ii}	0.76 (2)	1.91 (3)	2.6663 (15)	174 (2)
O1—H2O···O3^{iii}	0.76 (2)	1.94 (2)	2.6956 (15)	175 (2)

Symmetry codes: (ii) $-x, y-1, -z+\frac{1}{2}$; (iii) $-x, -y, -z$.

Table 3
Selected geometric parameters (Å, °) for (I) at 250 K.

Zn1—O1	2.0027 (13)	O2—C1	1.261 (2)
Zn1—O2	2.1904 (15)	O3—C1	1.257 (2)
Zn1—O3	2.1911 (12)		
O1—Zn1—O1^{i}	98.70 (8)	O1—Zn1—O2^{i}	96.05 (6)
O1—Zn1—O3^{i}	105.96 (6)	O2—Zn1—O3^{i}	101.74 (5)
O1—Zn1—O3	89.97 (5)	O2^{i}—Zn1—O2	85.37 (7)
O3^{i}—Zn1—O3	155.68 (8)	C1—O2—Zn1	91.13 (11)
O1—Zn1—O2	148.47 (5)	C1—O3—Zn1	91.22 (10)
O2—Zn1—O3	59.13 (5)	O3—C1—O2	118.33 (16)

Symmetry code: (i) $-x, y, -z+\frac{1}{2}$.

Table 4
Hydrogen-bond geometry (Å, °) for (I) at 250 K.

D—H···A	D—H	H···A	D···A	D—H···A
O1—H1O···O2^{ii}	0.69 (3)	1.98 (3)	2.6702 (19)	169 (3)
O1—H2O···O3^{iii}	0.78 (3)	1.92 (3)	2.7023 (18)	175 (2)

Symmetry codes: (ii) $-x, y-1, -z+\frac{1}{2}$; (iii) $-x, -y, -z$.

Compound (I) at 250 K, (I*b*)

Crystal data

$[Zn(C_2H_3O_2)_2(H_2O)_2]$
M_r = 219.49
Monoclinic, $C2/c$
a = 14.2904 (5) Å
b = 5.34245 (11) Å
c = 10.9616 (2) Å
β = 99.590 (1)°
V = 825.17 (4) Å^3
Z = 4
Mo $K\alpha$ radiation
μ = 2.96 mm^{-1}
T = 250 (2) K
0.42 × 0.30 × 0.06 mm

Data collection

Nonius KappaCCD area-detector diffractometer
Absorption correction: numerical (*SADABS*; Sheldrick, 2008*a*)
T_{min} = 0.405, T_{max} = 0.864
6929 measured reflections
940 independent reflections
888 reflections with $I > 2\sigma(I)$
R_{int} = 0.017

Refinement

$R[F^2 > 2\sigma(F^2)]$ = 0.020
$wR(F^2)$ = 0.056
S = 1.10
940 reflections
60 parameters
H atoms treated by a mixture of independent and constrained refinement
$\Delta\rho_{max}$ = 0.29 e Å^{-3}
$\Delta\rho_{min}$ = −0.30 e Å^{-3}

Because many effects discussed in this paper might be influenced by the correctness of the absorption correction, special care was taken to index the crystal faces and measure their distances. This information was used for the numerical absorption correction in the program *SADABS* (Sheldrick, 2008*a*), which additionally refines spherical harmonics functions based on multiple measured reflections to improve further the reliability of the data.

The O-bound H atoms of the water molecule were located in a difference Fourier map and refined freely with isotropic displacement parameters. The difference density map in the plane of the methyl H atoms does not show distinct maxima. The methyl H atoms were therefore introduced in calculated positions and refined with C—H = 0.97–0.98 Å and U_{iso}(H) = 1.5U_{eq}(C) using a large number of refinement cycles.

For both determinations, data collection: *COLLECT* (Nonius, 1999); cell refinement: *PEAKREF* (Schreurs, 2008); data reduction:

Table 5
Hirshfeld rigid-bond test (Hirshfeld, 1976) of the Zn—O(carboxylate) bonds: comparison of (I*a*), (I*b*) and ZNAQAC03 (Ishioka *et al.*, 1997) with zinc carboxylate structures extracted from *Acta Crystallographica*.

The structures are identified by their refcode in the Cambridge Structural Database (Allen, 2002). Only the maximum m.s.d.a. values are given.

CSD refcode	Zn site symmetry	T (K)	Δ m.s.d.a. (Å^2)	Δ m.s.d.a./σ
(I*a*)	2	110	0.0080 (5)	16.06
(I*b*)	2	250	0.0221 (7)	31.62
ZNAQAC03	2	292	0.0272 (25)	10.87
ACOGIJ01	1	298	0.0141 (12)	11.72
CEHCAT01	2	160	0.0047 (9)	5.18
CICHOM	2	293	0.0276 (12)	22.99
EDUNOH	2	292	0.0050 (9)	5.61
EXOZUM	1	293	0.0260 (27)	9.62
EYOVOD	1	293	0.0276 (19)	14.55
EYOVUJ	1	293	0.0102 (17)	6.01
FERQID	1	293	0.0244 (8)	30.48
GAVPAV	1	295	0.0350 (37)	9.47
GETZOV	1	293	0.0134 (24)	5.58
GIMHUG	1	263	0.0133 (30)	4.43
HAMMOY	1	293	0.0368 (14)	26.30
HAYTOR	1	295	0.0357 (14)	25.49
HAYXIP	1	234	0.0120 (14)	8.57
HIQDIV	1	295	0.0046 (8)	5.81
HIQSUW	1	293	0.0174 (14)	12.44
KIWNOU	2	294	0.0109 (27)	4.04
KIWNUA	1	294	0.0448 (16)	27.97
KIYSEQ	2	299	0.0151 (17)	8.91
JEWDIZ	1	293	0.0090 (8)	11.19
NEQLIF	1	298	0.0122 (34)	3.59
NIWNOX	1	295	0.0101 (14)	7.22
PAHSOH	1	293	0.0289 (18)	16.03
PESKEE	1	153	0.0208 (50)	4.16
REHDIS	1	292	0.0191 (23)	8.29
VAVFUU02	1	298	0.0279 (34)	8.21
VIQLEN	1	293	0.0275 (17)	16.20
WEJMOO	1	292	0.0103 (17)	6.07
WIZRAZ	1	293	0.0596 (20)	29.80
XIYJAR	1	298	0.0104 (18)	5.80
XIYJEV	1	296	0.0125 (15)	8.32
XIYNOJ	1	296	0.0251 (14)	17.94
YASMOV	1	295	0.0211 (16)	13.19

Structures FAXPEA and UMIBIB have been omitted because of disorder.

Table 6
Tensor components of the thermal expansion (10^{-6} K^{-1}) in the Cartesian *xyz* coordinate system (α_{12}, α_{23} = 0).

T (K)	α_{11}	α_{22}	α_{33}	α_{13}
290–270	171.83	−25.03	26.38	−66.61
270–250	169.18	−33.16	23.65	−71.36
250–230	174.96	−26.40	25.26	−88.10
230–210	177.31	−44.72	27.88	−93.61
210–190	178.82	−33.66	19.71	−98.09
190–170	174.93	−29.99	41.78	−80.03
170–150	189.30	−75.00	18.95	−143.43
150–130	199.49	−71.55	37.89	−146.19
130–110	228.14	−79.43	7.33	−178.73

PIXEL15 (Xian *et al.*, 2006) and *SADABS* (Sheldrick, 2008*a*); method used to solve structure: initial coordinates from Ishioka *et al.* (1997); program(s) used to refine structure: *SHELXL97* (Sheldrick, 2008*b*); molecular graphics: *PLATON* (Spek, 2003); software used to prepare material for publication: *SHELXL97*.

This work was supported by the Council for Chemical Sciences of the Netherlands Organization for Scientific Research (CW–NWO).

Table 7
Eigenvalues (10^{-6} K^{-1}) of the thermal expansion tensor and angles of the eigenvectors with the crystallographic axes.

T (K)	Principal axis	Eigenvalue	Angle with **a**	Angle with **b**	Angle with **c**
290–270	α_1	198 (3)	11.5 (5)	90	111.2 (5)
	α_2	0(3)	78.5 (5)	90	21.2 (5)
	α_3	−25 (4)	90	180	90
270–250	α_1	198 (3)	12.6 (5)	90	112.2 (5)
	α_2	−6(2)	77.4 (5)	90	22.2 (5)
	α_3	−33 (4)	90	180	90
250–230	α_1	216 (4)	15.4 (5)	90	114.8 (5)
	α_2	−15 (3)	74.6 (5)	90	24.8 (5)
	α_3	−26 (4)	90	180	90
230–210	α_1	222 (4)	16.4 (6)	90	115.7 (6)
	α_2	−17 (4)	73.6 (6)	90	25.7 (6)
	α_3	−44 (4)	90	180	90
210–190	α_1	226 (4)	16.4 (5)	90	115.5 (5)
	α_2	−27 (4)	73.6 (5)	90	25.5 (5)
	α_3	−34 (4)	90	180	90
190–170	α_1	213 (4)	16.2 (7)	90	115.1 (7)
	α_2	4(4)	73.8 (7)	90	25.1 (7)
	α_3	−30 (5)	90	180	90
170–150	α_1	271 (3)	21.0 (5)	90	119.7 (5)
	α_2	−62 (4)	69.0 (5)	90	29.7 (5)
	α_3	−75 (4)	90	180	90
150–130	α_1	286 (3)	22.2 (5)	90	120.5 (5)
	α_2	−48 (4)	67.8 (5)	90	30.5 (5)
	α_3	−72 (4)	90	180	90
130–110	α_1	328 (4)	21.2 (4)	90	119.2 (4)
	α_2	−79 (4)	90	0	90
	α_3	−92 (4)	68.8 (4)	90	29.2 (4)

Table 8
Scale factor K = [mean(F_o^2)/mean(F_c^2)] versus intensity for (I*a*).

F_c/F_c(max)	Number of reflections	K
<0.039	94	1.050
<0.076	91	1.020
<0.110	94	0.996
<0.140	91	0.985
<0.170	94	0.999
<0.200	92	0.999
<0.241	91	1.006
<0.304	94	1.000
<0.413	91	1.004
<1.000	93	1.000

Supplementary data for this paper are available from the IUCr electronic archives (Reference: GZ3157). Services for accessing these data are described at the back of the journal.

References

Allen, F. H. (2002). *Acta Cryst.* B**58**, 380–388.
Altomare, A., Burla, M. C., Camalli, M., Cascarano, G. L., Giacovazzo, C., Guagliardi, A., Moliterni, A. G. G., Polidori, G. & Spagna, R. (1999). *J. Appl. Cryst.* **32**, 115–119.
Clegg, W., Little, I. R. & Straughan, B. P. (1986). *Acta Cryst.* C**42**, 1701–1703.
Dietzel, P. D. C., Blom, R. & Fjellvåg, H. (2006). *Dalton Trans.* pp. 586–593.
Duisenberg, A. J. M., Hooft, R. W. W., Schreurs, A. M. M. & Kroon, J. (2000). *J. Appl. Cryst.* **33**, 893–898.
Farrugia, L. J. (1999). *J. Appl. Cryst.* **32**, 837–838.
Hirshfeld, F. L. (1976). *Acta Cryst.* A**32**, 239–244.
Hummel, W., Hauser, J. & Bürgi, H.-B. (1990). *J. Mol. Graph.* **8**, 214–220.
Ishioka, T., Murata, A., Kitagawa, Y. & Nakamura, K. T. (1997). *Acta Cryst.* C**53**, 1029–1031.
Ishioka, T., Shibata, Y., Takahashi, M., Kanesaka, I., Kitagawa, Y. & Nakamura, K. T. (1998). *Spectrochim. Acta A*, **54**, 1827–1836.

Kaduk, J. A. & Chen, Y.-M. (1996). Private communication (refcode ZNAQAC02). CCDC, Union Road, Cambridge, England.
Küppers, H. (2003). *Thermal Expansion*. *International Tables for Crystallography*, Vol. D, *Physical Properties of Crystals*, 1st ed., edited by A. Authier, ch. 1.4, pp. 99–104. Heidelberg: Springer.
Niekerk, J. N. van, Schoening, F. R. L. & Talbot, J. H. (1953). *Acta Cryst.* **6**, 720–723.
Nonius (1999). *COLLECT*. Nonius BV, Delft, The Netherlands.
Ohashi, Y. (1982). Source code for *STRAIN* available in *Comparative Crystal Chemistry*, by R. M. Hazen & L. W. Finger, pp. 92–102. Chichester: Wiley-Interscience.
Palatinus, L. & van der Lee, A. (2008). *J. Appl. Cryst.* **41**, 975–984.
Robinson, K., Gibbs, G. V. & Ribbe, P. H. (1971). *Science*, **172**, 567–570.
Salud, J., Barrio, M., López, D. O., Tamarit, J. L. & Alcobé, X. (1998). *J. Appl. Cryst.* **31**, 748–757.
Schomaker, V. & Trueblood, K. N. (1998). *Acta Cryst.* B**54**, 507–514.
Schreurs, A. M. M. (2008). *PEAKREF*. University of Utrecht, The Netherlands.
Semenenko, K. N. & Kurdyumov, G. M. (1958). *Vestn. Mosk. Univ. Ser. Mat. Mekh. Astron. Fiz. Khim.* **13**, 207–209.
Sheldrick, G. M. (2008*a*). *SADABS*. Version 2008/1. University of Göttingen, Germany.
Sheldrick, G. M. (2008*b*). *Acta Cryst.* A**64**, 112–122.
Spek, A. L. (2003). *J. Appl. Cryst.* **36**, 7–13.
Tao, J., Tong, M.-L., Shi, J.-X., Chen, X.-M. & Ng, S. W. (2000). *Chem. Commun.* pp. 2043–2044.
Walker, M., Pohl, E., Herbst-Irmer, R., Gerlitz, M., Rohr, J. & Sheldrick, G. M. (1999). *Acta Cryst.* B**55**, 607–616.
Xian, X., Schreurs, A. M. M. & Kroon-Batenburg, L. M. J. (2006). *Acta Cryst.* A**62**, s92.